2016

Head Wave Correlations in Ambient Noise

John Thomas Gebbie
Metron Scientific Solutions, john.gebbie@gmail.com

Martin Siderius
Portland State University, siderius@pdx.edu

Head wave correlations in ambient noise

John Gebbie[a)]

Metron Scientific Solutions, 1900 Southwest 4th Avenue, Suite 89-01,
Portland, Oregon, 97201, USA
gebbie@metsci.com

Martin Siderius

Northwest Electromagnetics and Acoustics Research Laboratory,
Department of Electrical and Computer Engineering, Portland State University,
1900 Southwest 4th Avenue, Suite 160, Portland, Oregon 97201, USA
siderius@pdx.edu

Abstract: Ambient ocean noise is processed with a vertical line array to reveal coherent time-separated arrivals suggesting the presence of head wave multipath propagation. Head waves, which are critically propagating water waves created by seabed waves traveling parallel to the water-sediment interface, can propagate faster than water-only waves. Such eigenrays are much weaker than water-only eigenrays, and are often completely overshadowed by them. Surface-generated noise is different whereby it amplifies the coherence between head waves and critically propagating water-only waves, which is measured by cross-correlating critically steered beams. This phenomenon is demonstrated both experimentally and with a full wave simulation.

1. Introduction

A passive fathometer method[1] was recently demonstrated in which seabed reflections of surface-generated ambient noise were detected using a vertical line array (VLA). In that technique, two beams were steered in the opposite end fire directions to isolate noise traveling toward and away from the seabed. Cross correlation yielded a fathometer-like return showing a pulse on the time axis offset by the two-way travel time to the seabed. In this article, the same basic two-beam correlation processing is applied to ambient noise data collected in the Mediterranean Sea in 2003, but the beams are instead steered at the positive and negative critical angle of the seabed. Correlation pulses appear at time offsets that are theoretically consistent with the seabed splitting critically incident waves into reflected waves and head waves, where the latter arrives first due to faster propagation through the seabed.

Head waves have been extensively studied in the field of seismology,[2] where they are used to model acoustic propagation through the Earth's layers. Oceanic sources can also cause head waves at the water-sediment interface.[3] Recent studies involving explosive sources examined the differences between head waves and precursor arrivals,[4] where the latter are waves that undergo upward refraction in the seabed. In terms of ambient noise, head waves have been observed affecting the spectral composition at very low frequencies using geophones.[5]

Consider a point source that produces a spherically spreading wave in a simple waveguide, as depicted in Fig. 1. This diagram shows the different wavefronts emanating from a point source. Inside the critical range, where the incident ray is above the critical angle, the direct wave splits into reflected and transmitted waves.[7] Beyond the critical range, the direct wave is totally reflected. However, at the critical range, where the incident ray is exactly at the critical angle, the transmitted wave travels parallel to the interface. This part of the transmitted wave is the so-called lateral wave. As the lateral wave propagates in the seabed, it continually perturbs water particles on the interface. In the same way that elements of a linear transmitter array can be delayed to synthesize a flat wavefront, these perturbations superimpose to form a conical water-borne wavefront. This is the head wave (HW), and it propagates in the water at exactly the critical angle. This article looks at the signal coherence between the HW and the part of the reflected wave that exists only at the critical angle, or critically reflected wave (CRW). Both propagate at the critical angle but become separated in

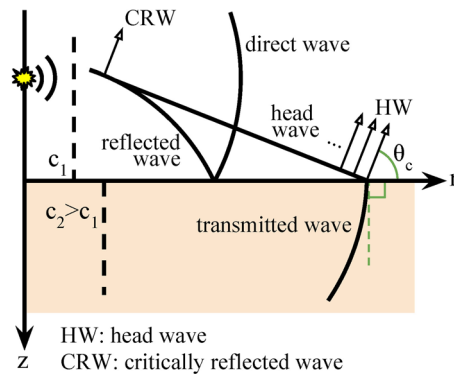[a)]Author to whom correspondence should be addressed.

Fig. 1. (Color online) Schematic of a head wave. Adapted from Jensen, 2011 (Ref. 6).

range because the lateral wave that creates the HW propagates faster than the CRW. This separation in range manifests as a separation in time, as observed by a fixed receiver. Cross-correlating critically steered beams exposes this separation.

2. Modeling correlated arrivals

The arrival directions and the time separation between the HW and CRW can be determined using ray theory. This is accomplished by finding a pair of eigenrays that start at the point on the seabed where the incident ray splits, and ends at the receiver. Ray theory is the physical model used in this analysis, but special treatment is needed for the conically shaped HW eigenray. The water column is assumed to have a constant velocity, and the seabed is a half space. Each point on a spherical wavefront corresponds to a ray traveling in a unique direction, but the same is not true for a conical wave. The HW phenomenon is often depicted as an incident ray entering the seabed at the critical angle, traveling horizontally for an arbitrary distance, and then being relaunched back into the water as a HW traveling at the critical angle. In fact, the HW can be thought of as being continually relaunched at every range beyond the critical range. This is because for single azimuth angle every point on the HW wavefront corresponds to a ray pointing in the same direction. Determining HW eigenrays requires accounting for a variable amount of horizontal travel through the seabed.

The time separation depends on the distance the HW eigenray travels through the seabed. Since the HW and CRW both propagate at the same angle in constant-velocity water, the time separation can also be determined using the difference in the amount of vertical travel of each eigenray. Let Δz_{HW} and Δz_{CRW} be the accumulated vertical travel distances of each of the paths, which are positive quantities. The time separation is then

$$\tau = \frac{\Delta z_{CRW} - \Delta z_{HW}}{c_w} \sin \theta_c, \tag{1}$$

where c_w is the sound speed of the water.

There are four fundamental HW-CRW eigenray pairs that are observable with the VLA. A fundamental eigenray pair is where the CRW eigenray undergoes one additional boundary reflection. Figure 2(a) shows paths where the CRW and HW come from opposite directions, and is referred to as the "conjugate-cross-beam" case. Figure 2(b) shows paths where the CRW and HW arrive on the same side, called the "auto-beam" case. For Fig. 2(a), using the surface-steered beam as a reference, the observed arrival time differences are $\tau = -(2z_r/c_w) \sin \theta_c$ and $\tau = [2(z_b - z_r)/c_w] \sin \theta_c$ for the left and right sides, respectively. For Fig. 2(b), the time delay is $\tau = \pm(2z_b/c_w) \sin \theta_c$. The surface-steered beam is chosen as the reference beam such that signals that arrive later in time on the seabed-steered beam appear on the positive side of the time axis, which is consistent with a fathometer. Longer eigenray pairs can be constructed by appending additional full water column cycles to each fundamental path [corresponding to the triangles in Fig. 2(b)], which corresponds to adding multiples of $\pm(2z_b/c_w) \sin \theta_c$ to τ.

3. Simulation

Numerical simulation can be used to confirm the noise correlations in time and angle. The theoretical model used here for the ambient noise due to surface breaking waves is developed using wavenumber integration.[8,9] This was implemented numerically in the OASN feature in the Ocean Acoustic and Seismic Exploration Synthesis (OASES)
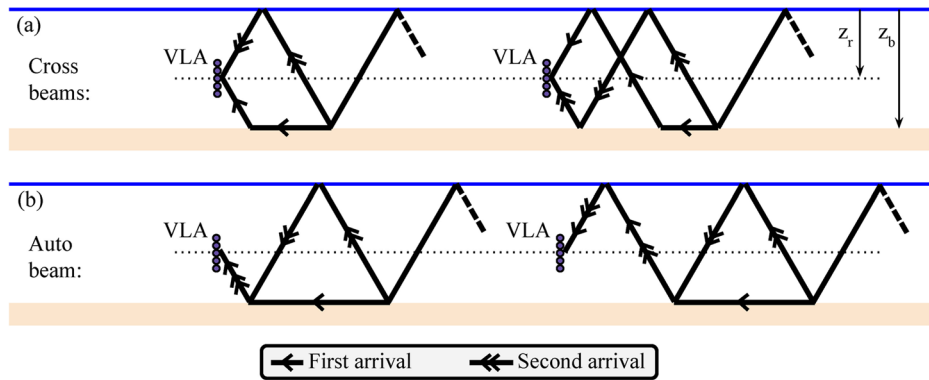
Fig. 2. (Color online) Ray diagram showing paths that produce correlation pulses.

package.[10] This model assumes breaking waves can be represented as a uniform distribution of randomly excited point sources located a fraction of a wavelength from the sea-surface.

The pressure field at angular frequency ω [adopting an $\exp(-i\omega t)$ convention] can be written as a column vector $\mathbf{p} = [p_1, p_2, ..., p_M]$ for M hydrophones. For conventional beamforming (i.e., delay and sum), the weight for the mth hydrophone steered at angle θ for plane waves arriving at grazing angle θ between the hydrophones separated by distance d is written,

$$w_m = e^{-imkd\sin\theta}. \tag{2}$$

The array is referenced to the shallowest hydrophone which is element $m = 0$. The wavenumber is $k = \omega/c$ and c is the sound speed in the water (1500 m/s). Writing the steering weights as a column vector, $\mathbf{w} = [w_0, w_1, ..., w_{M-1}]$, the beam, $b(\theta)$, is written

$$b(\theta) = \mathbf{w}^\dagger \mathbf{p}, \tag{3}$$

where the dagger represents the conjugate transpose operation. The conventional instantaneous beam power for a given direction θ is computed by the following:

$$B_a(\theta) = \mathbb{E}[\mathbf{w}^\dagger \mathbf{p}(\mathbf{w}^\dagger \mathbf{p})^\dagger] = \mathbb{E}[\mathbf{w}^\dagger \mathbf{p}\mathbf{p}^\dagger \mathbf{w}] = \mathbf{w}^\dagger \mathbb{E}[\mathbf{p}\mathbf{p}^\dagger]\mathbf{w} = \mathbf{w}^\dagger \mathbf{K}\mathbf{w}, \tag{4}$$

where $\mathbb{E}[\cdots]$ is the expected value operator and $\mathbf{K}$ is the cross-spectral density matrix (CSDM).

The OASN model produces a synthetic cross-spectral density matrix $\mathbf{K}$ which is exact (to numerical accuracy) and is sometimes referred to as the clairvoyant CSDM. This is in contrast to the sample-averaged CSDM which is used with measured data and described in Sec. 4.

To obtain the time-domain auto-beam correlation [as shown in Fig. 2(b)] the frequency dependent beam output is Fourier transformed,

$$C_a(t, \theta) = \mathcal{F}^{-1}\{B_a(\omega, \theta)\}. \tag{5}$$

The conjugate-cross-beam correlation [as shown in Fig. 2(a)] is nearly the same as the auto-beam but with the weight vector conjugated $\mathbf{w}^*$ such that the conjugate-cross-beam correlation is

$$B_c(\theta) = \mathbf{w}^\dagger \mathbf{K}\mathbf{w}^*, \tag{6}$$

and the time-domain conjugate-cross-beam correlation

$$C_c(t, \theta) = \mathcal{F}^{-1}\{B_c(\omega, \theta)\}. \tag{7}$$

The description above is for delay and sum beamforming but often adaptive beam forming produces superior results.[11,12] The analysis that follows used adaptive methods but similar results were observed even for delay and sum beamforming.

A simulation was performed using OASN for the following waveguide parameters: Iso-speed water column of 1500 m/s, infinite half-space seabed with sound speed 1530 m/s, density 1.5 g/cm^3, and attenuation of 0.75 decibels per wavelength. The model was computed every 0.25 Hz over the band 3400–4000 Hz. The response was computed on a 32 hydrophone array with 0.18 m spacing located at a depth of 73 m (depth of the top hydrophone) with the total water depth being 133 m. The output from the model was $\mathbf{K}$ at each frequency and these simulated data were beamformed
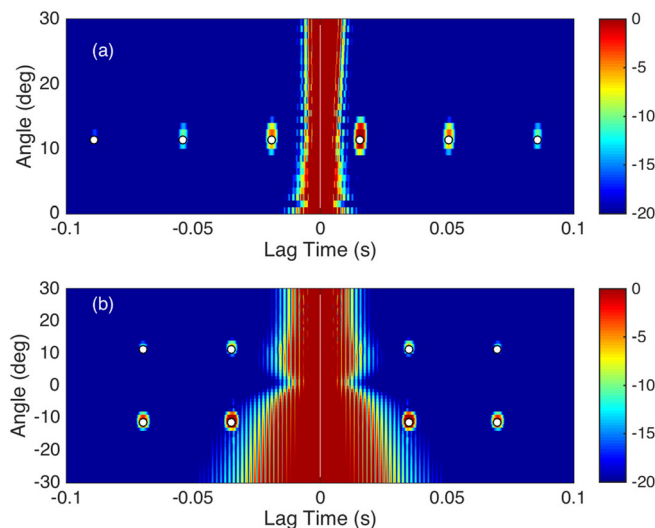
Fig. 3. (Color online) OASES simulation of beam correlations normalized on a decibel scale. Top panel (a) shows conjugate-cross-correlated beams for angles from $0°$–$30°$. Lower panel shows auto-correlated beams from $0°$–$\pm30°$. The negative lag-times indicate correlations where the upward traveling wave is ahead of the downward traveling wave and positive lag-times are for the opposite. The white circles are the predicted angle/lag-times.

for angles from $0°$–$90°$ for the conjugate-cross-beams B_c and from $0°$–$180°$ for the auto-beams B_a. The time-domain correlations are shown in Fig. 3 where the conjugate-cross-beams $C_c(t, \theta)$ is shown in panel (a) and the auto-beams $C_a(t, \theta)$ is in panel (b). The figure also has white dots that show the time and angles for the predicted beam correlations. Note, the correlations occur near $10°$ which corresponds to the critical angle of the seabed and the propagation direction for the head wave.

4. Experiment

To examine the existence of the beam correlations, the same procedure as outlined in Sec. 3 was applied to experimental data. The data used were taken from the Boundary 2003 experiment[13] conducted by the NATO Centre for Maritime Research and Experimentation (formerly the NATO Undersea Research Centre). The array used had 32 hydrophones uniformly spaced at 0.18 m apart and was vertically oriented in the water column. The array was drifting slowly hence the averaging time was limited to a few minutes to avoid too large a change in the environment over the averaging time. The data were collected in the band from 20 to 4000 Hz but for this analysis the band from 3400 to 4000 Hz was used as was done for the modeling simulations shown
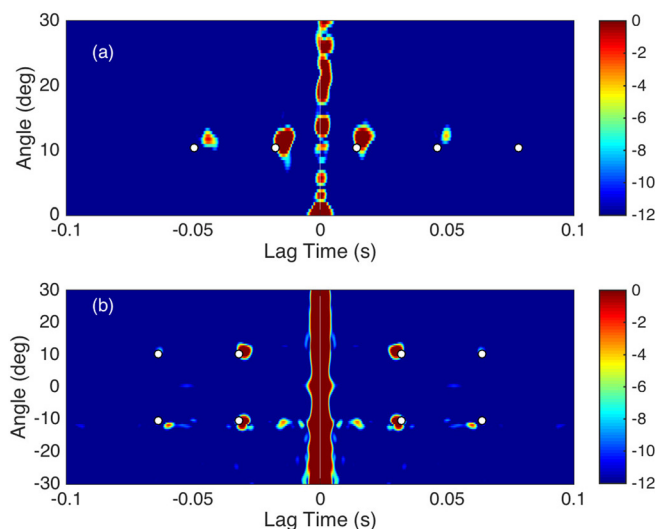

Fig. 4. (Color online) Beam cross and auto-correlations for measured data. This plot is similar to Fig. 3 but with results taken from the Boundary03 data set.

previously in Fig. 3. The array was roughly positioned with the first hydrophone at a depth of approximately 73 m and the water depth 133 m.

The data were processed taking time samples corresponding to 0.34 s (i.e., a snapshot length) on each channel and using a fast Fourier transform to obtain the frequency domain pressure field vector. The CSDM was computed by the outer product of the pressure vector data followed by averaging over approximately 585 snapshots (around 3.3 min). This produces an estimated CSDM $\hat{\mathbf{K}}$.

The results of the cross- and auto-correlated beams is shown in Fig. 4. The white dots in this figure come from the same parameters used to generate Fig. 3, which assume a constant sound speed in the water. Small deviations from peaks in the data may be due to unaccounted for refraction effects in the water column.

5. Conclusion

The time offsets and angles of peaks that appear when cross-correlating critically steered beams indicate that the ocean ambient noise field is exciting head waves that can be detected. Evidence of this is prominent in both experimental data and in a full-wave simulation. Since any critically incident wave on the seabed will split into two parts that propagate at different speeds, which leads to a time separation at a receiver, an area of future investigation is to determine the composition of the critically incident energy in terms of how much is due to conical waves emitted from the seabed at distant ranges. Measured time separations of arrivals are strongly dependent on the critical angle of the seabed, and information garnered from this technique may provide a new means of estimating seabed geoacoustic properties.

Acknowledgments

References and links

[1] M. Siderius, C. H. Harrison, and M. B. Porter, "A passive fathometer technique for imaging seabed layering using ambient noise," J. Acoust. Soc. Am. **120**, 1315–1323 (2006).

[2] K. Aki and P. G. Richards, *Quantitative Seismology*, 2nd ed. (University Science Books, Sausalito, CA, 2009).

[3] L. M. Brekhovskikh, "Reflection and refraction of spherical waves," in *Waves in Layered Media*, 2nd ed. (Academic Press, New York, 1980), Chap. 4, pp. 225–298.

[4] P. H. Dahl and J. W. Choi, "Precursor arrivals in the yellow sea, their distinction from first-order head waves, and their geoacoustic inversion," J. Acoust. Soc. Am. **120**, 3525–3533 (2006).

[5] H. Schmidt and W. A. Kuperman, "Estimation of surface noise source level from low-frequency seismoacoustic ambient noise measurements," J. Acoust. Soc. Am. **84**, 2153–2162 (1988).

[6] F. B. Jensen, W. A. Kuperman, M. B. Porter, and H. Schmidt, "Broadband modeling," in *Computational Ocean Acoustics*, edited by W. M. Hartmann, 2nd ed. (Springer, New York, 2011), Chap. 8, pp. 611–660.

[7] F. B. Jensen, W. A. Kuperman, M. B. Porter, and H. Schmidt, "Wave propagation theory," in *Computational Ocean Acoustics*, edited by W. M. Hartmann, 2nd edition (Springer, New York, 2011), Chap. 2, pp. 65–153.

[8] W. A. Kuperman and F. Ingenito, "Spatial correlation of surface generated noise in a stratified ocean," J. Acoust. Soc. Am. **67**, 1988–1996 (1980).

[9] H. Schmidt and F. B. Jensen, "A full wave solution for propagation in multilayered viscoelastic media with application to Gaussian beam reflection at fluid-solid interfaces," J. Acoust. Soc. Am. **77**, 813–825 (1985).

[10] H. Schmidt, *OASES User Guide and Reference Manual*, Department of Ocean Engineering at Massachusetts Institute of Technology, Cambridge, MA http://oceanai.mit.edu/lamss/pmwiki/pmwiki.php?n=Site.Oases, 3.1 edition (2004) (Last viewed 26 June 2016).

[11] M. Siderius, H. Song, P. Gerstoft, W. S. Hodgkiss, P. Hursky, and C. Harrison, "Adaptive passive fathometer processing," J. Acoust. Soc. Am. **127**, 2193–2200 (2010).

[12] P. Gerstoft, W. S. Hodgkiss, M. Siderius, C.-F. Huang, and C. H. Harrison, "Passive fathometer processing," J. Acoust. Soc. Am. **123**, 1297–1305 (2008).

[13] C. H. Harrison, "Performance and limitations of spectral factorization for ambient noise sub-bottom profiling," J. Acoust. Soc. Am. **118**, 2913–2923 (2005).